Supporting Information for

Visualizing spatial variations of plasmon-exciton polaritons at the nanoscale using electron microscopy

Andrew B. Yankovich[1], Battulga Munkhbat[1], Denis G. Baranov[1], Jorge Cuadra[1], Erik Olsén[1], Hugo Lourenço-Martins[2], Luiz H. G. Tizei[2], Mathieu Kociak[2], Eva Olsson[1,*], Timur Shegai[1,*]

1. *Department of Physics, Chalmers University of Technology, 412 96, Gothenburg, Sweden*
2. *Laboratoire de Physique des Solides, Univ. Paris-Sud, CNRS UMR 8502, Orsay, France*

* eva.olsson@chalmers.se; * timurs@chalmers.se

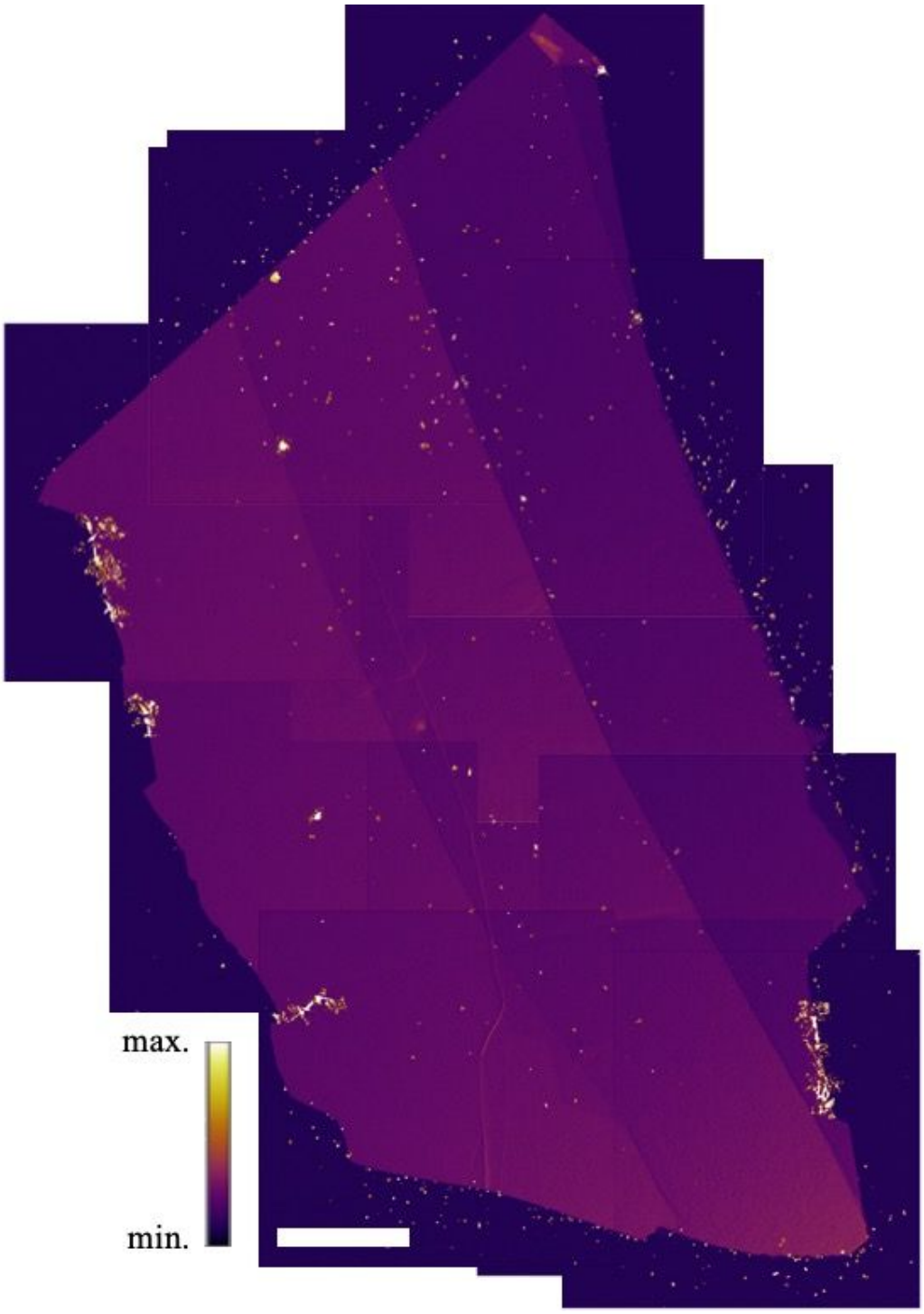

Figure S1. Low-magnification image of a hybrid system.
Composite HAADF STEM image that was created by overlaying multiple images of a coupled system, which is composed of a single WS_2 flake and Ag TNPs. The WS_2 flake has regions of different thickness, visible from the image contrast. The scale bar is 5 μm and the color scale is in arbitrary units.

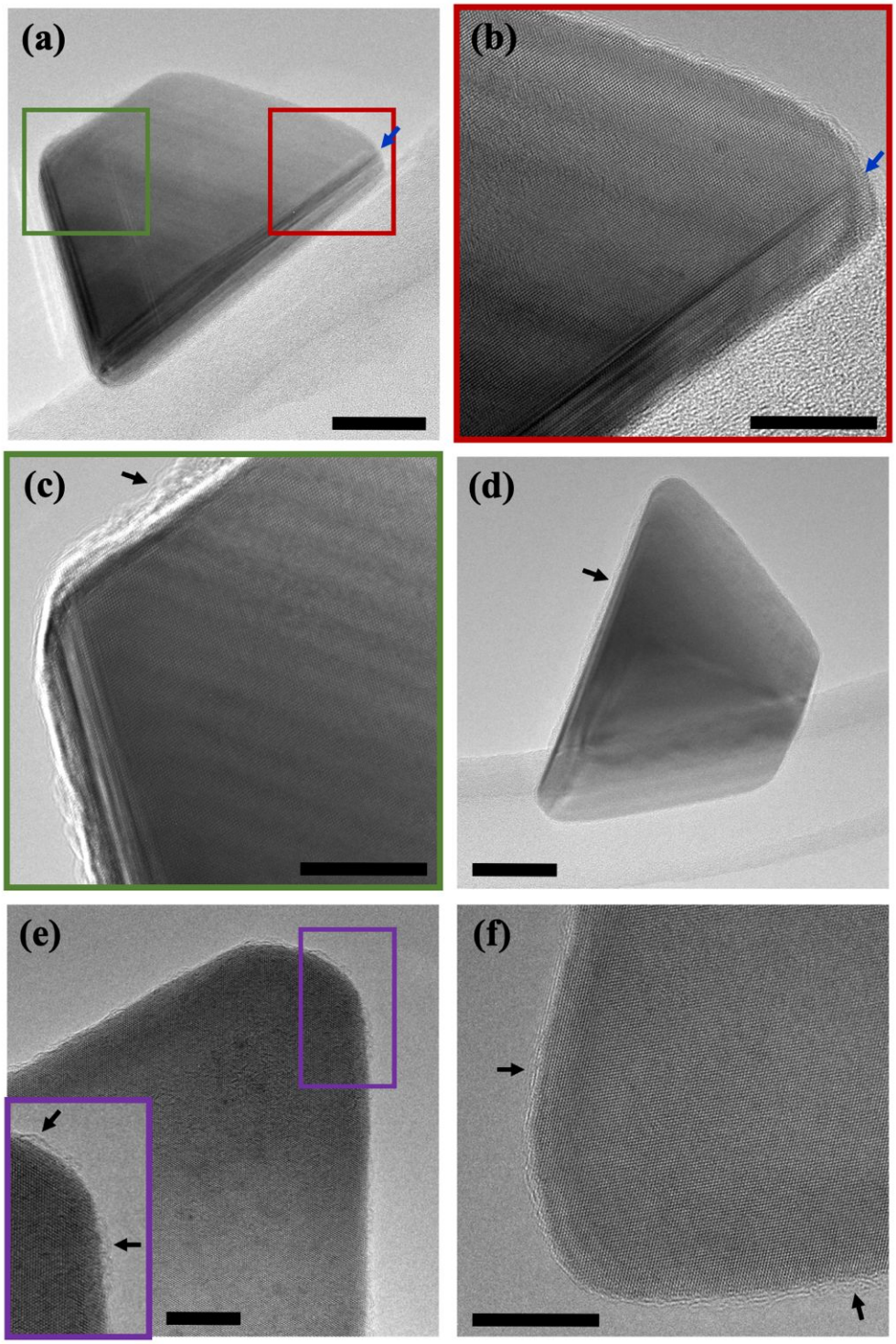

Figure S2. HRTEM images of Ag TNPs on an amorphous carbon support.
(a-d) Side-view HRTEM images of truncated TNPs, revealing the single crystal nature and clear faceted surfaces. (b) Enlarged HRTEM image of the red area in (a). A planar defect, which is likely a twin boundary, is marked in (a) and (b) by the blue arrows. These are the only type of crystalline defect observed in the TNPs. (c) Enlarged HRTEM image of the green area in (a). (d) HRTEM image of another typical TNP in side-view. (e) and (f) are top-view HRTEM images, again revealing the single crystal nature. The TNP ligand surface coating that is left over from the solution synthesis is marked in (c-f) by the black arrows. The coating thickness varies between 0 - 3 nm. The scale bars in (a-f) are 20, 10, 10, 30, 10, and 10 nm, respectively.

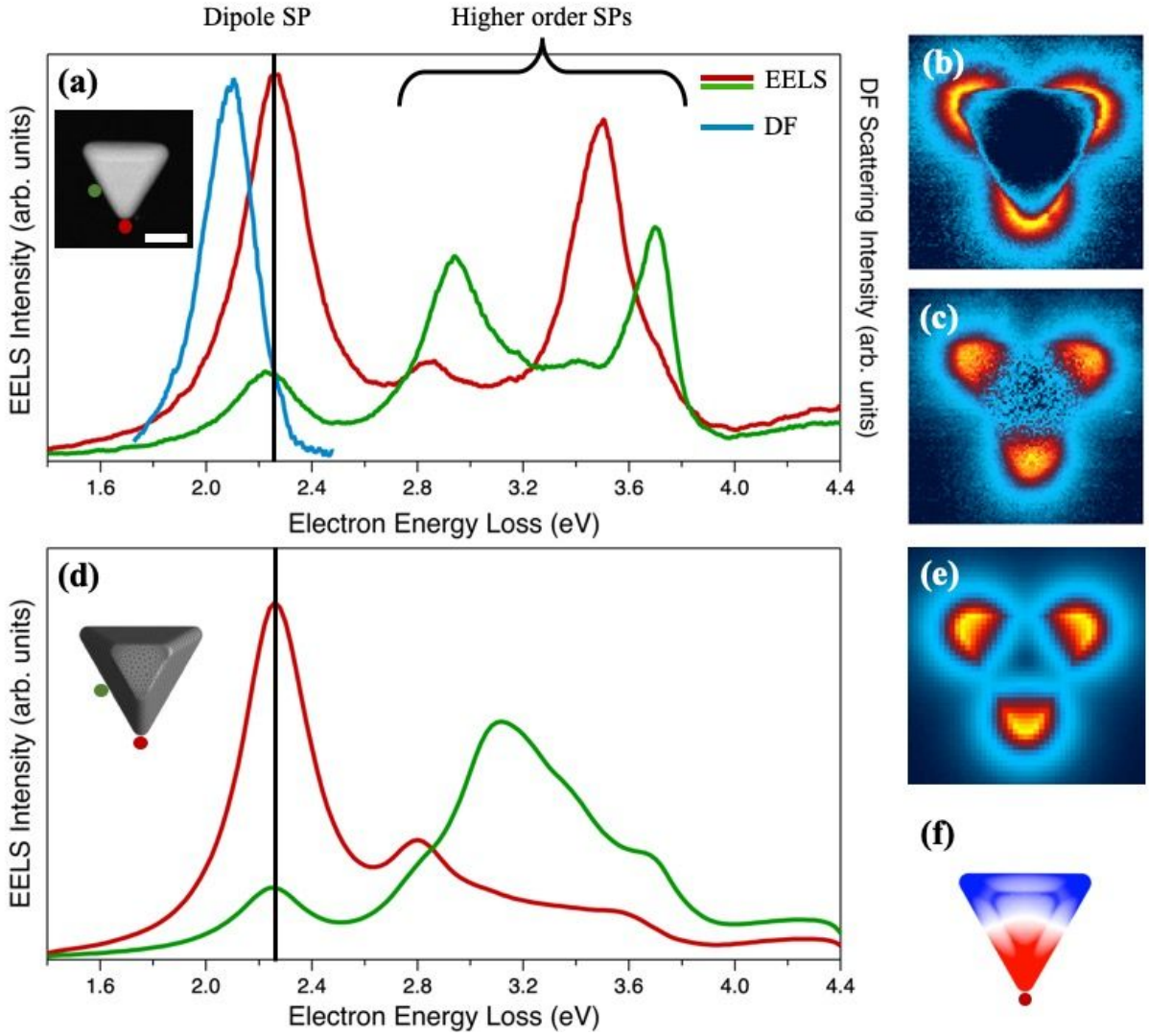

Figure S3. LSP modes of uncoupled TNPs.
(a) Experimental EELS and optical DF scattering spectra from the uncoupled Ag TNP on 20 nm Si_3N_4 shown in the inset HAADF STEM image. The scale bar is 50 nm. The red and green spectra are using electron beam positions identified by the colored markers in the inset image. The blue spectrum is the correlated DF scattering spectra. The lowest energy peak has the largest intensity and is the signal from the dipole LSP. The signals at higher energies are the higher order LSP modes. (b-c) Extracted maps at the dipole LSP peak position (2.26 eV marked by black line in (a)) from the (b) non-normalized and (c) normalized spectrum image of the same TNP shown in (a). (d) Simulated EELS spectra after a 70 meV broadening using a 100 nm TNP supported on 20 nm Si_3N_4. The red and green spectra are using electron beam positions identified by the colored markers in the inset model image, showing good agreement with the experimental dipole LSP, which is of interest in this study. There are differences in the higher order LSP EELS intensities, which likely show that the calculations do not fully capture the higher order LSP behavior that involve z directionality. (e) Simulated EELS map at the dipole LSP energy (2.26 eV marked by black line in (d)) showing excellent agreement with the normalized experimental map. (f) Simulated surface charge density distribution at 2.26 eV, revealing the dipole character.

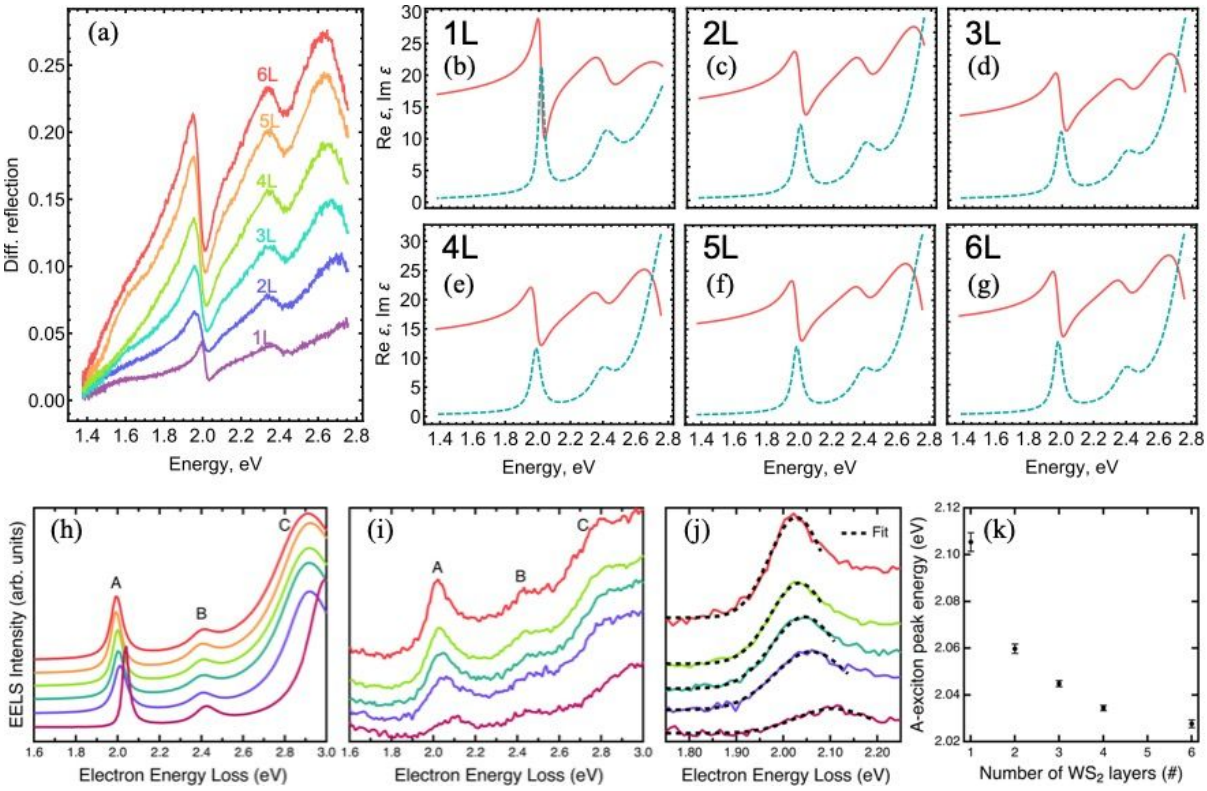

Figure S4. Thickness dependent optical and EELS signals of uncoupled WS_2.
(a) Measured optical differential reflectivity spectra R-R_{sub}, where R_{sub} is the reflection from the bare Si_3N_4 substrate, for WS_2 flakes of various thicknesses from 1 to 6 layers. The reflectivity data is from WS_2 flakes after plasma cleaning. The plasma cleaning reduces the extracted A-exciton oscillator strength from ~0.45 to ~0.35. (b)-(g) Permittivities of WS_2 flakes of various thicknesses extracted from the reflection spectra in (a) using the transfer matrix method (Methods). Solid and dashed lines show real and imaginary parts of the permittivities, respectively. (h) Simulated EELS spectra with no spectral broadening from experimental limitations for WS_2 flakes of various thicknesses from 1 to 6 layers utilizing the thickness-dependent permittivities in (b)-(g). The color labels are the same as in (a). (i) Experimental EELS spectra for WS_2 flakes of various thicknesses from 1 to 6 layers (5 layers in missing). The signals from the A, B, and C, excitons are clearly visible and agree with the simulated EELS signals. The origin of why the observed 1 layer WS_2 A-exciton signal is smaller than the theoretically predicted signal is unknown. (j) The same experimental spectra as in (h), but magnified around the A-exciton to show the shift in A-exciton position from different WS_2 thickness. The black dashed lines are Gaussian fits to each experimental A-exciton signal within the energy range displayed by the fit line. (k) Plot of the A-exciton peak position in EELS, defined here as the Gaussian fit peak position, as a function of number of WS_2 layers. The error bars are plus and minus the error in the fitted peak position, extracted directly from IGOR pro's automated fitting routine that utilizes the Levenberg–Marquardt L2-norm minimization method. A clear decrease in A-exciton position is observed in EELS with increasing the number of WS_2 layers, consistent with optical observations and theory.

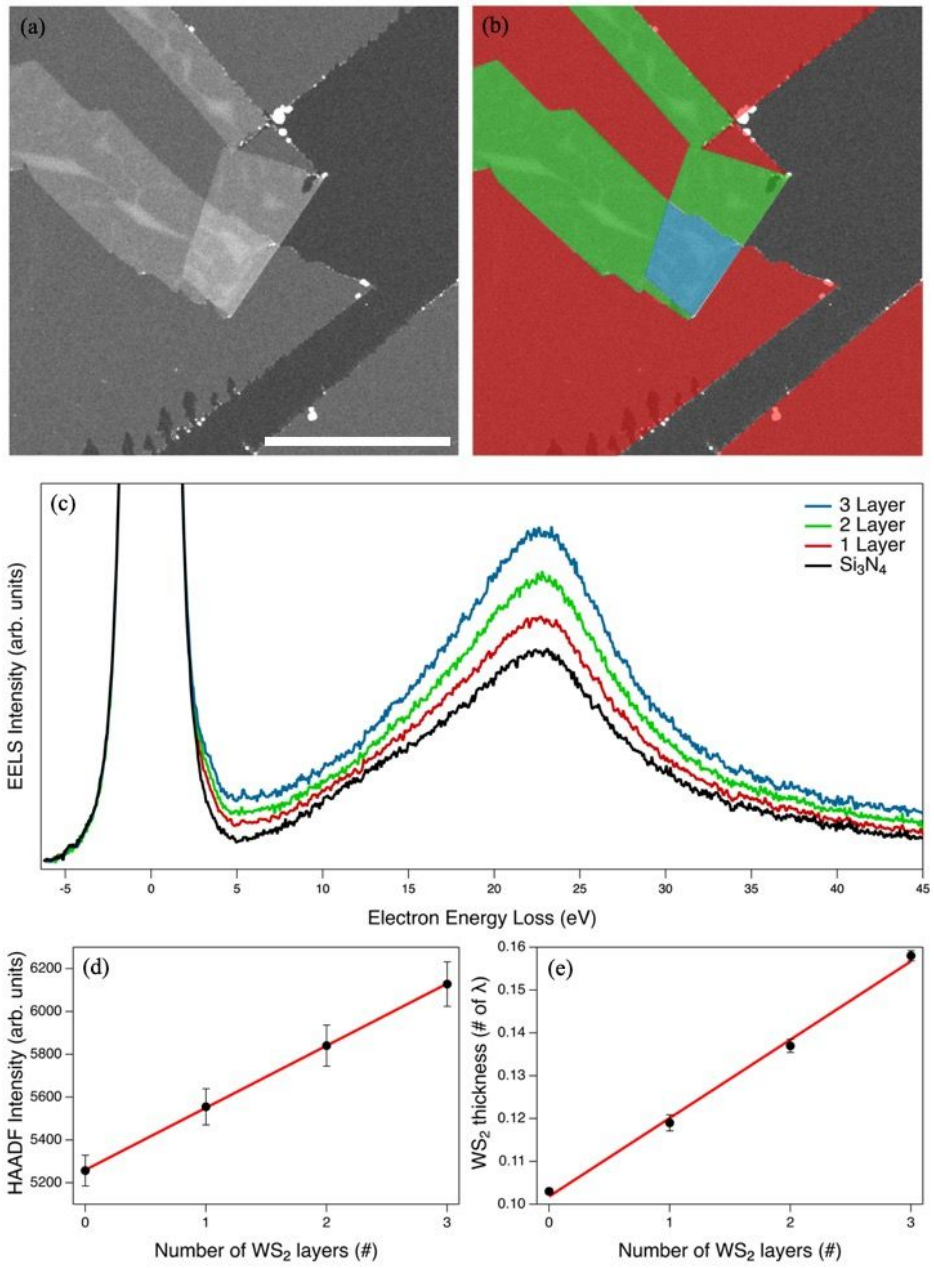

Figure S5. Calibrating WS_2 thickness measurements.
(a) HAADF STEM image of WS_2 reference flakes of known thickness between 0-3 layers. The scale bar is 1 μm. (b) The same image as (a) with Si_3N_4, 1 layer, 2 layers, and 3 layers regions marked by transparent, red, green, and blue shapes, respectively. (c) EELS spectra from the Si_3N_4, 1 layer, 2 layers, and 3 layers areas. The intensity axis range has been chosen to show the variations in the low-loss details and not the essentially identical zero-loss peaks. (d) Plot of the average HAADF STEM image intensity from different regions in (a) as a function of known number of WS_2 layers. The error bars represent plus and minus one standard deviation of the image intensity within the regions used to calculate the average intensities. (e) Plot of the measured WS_2 thickness in units of inelastic mean free paths (λ) as a function of known number of WS_2 layers. The thickness was measured using the EELS log-ratio method (Methods). Each data point represents the average of 3-5 different thickness measurements that were acquired from different regions within (a) but of the same WS_2 thickness. The error bars represent plus and minus one standard deviation of the 3-5 measurements. The red lines in (d) and (e) are linear fits of the data, showing a linear trend is observed for both thickness measurement methods. The calibrated linear fits were extrapolated to measure flakes of unknown thickness.

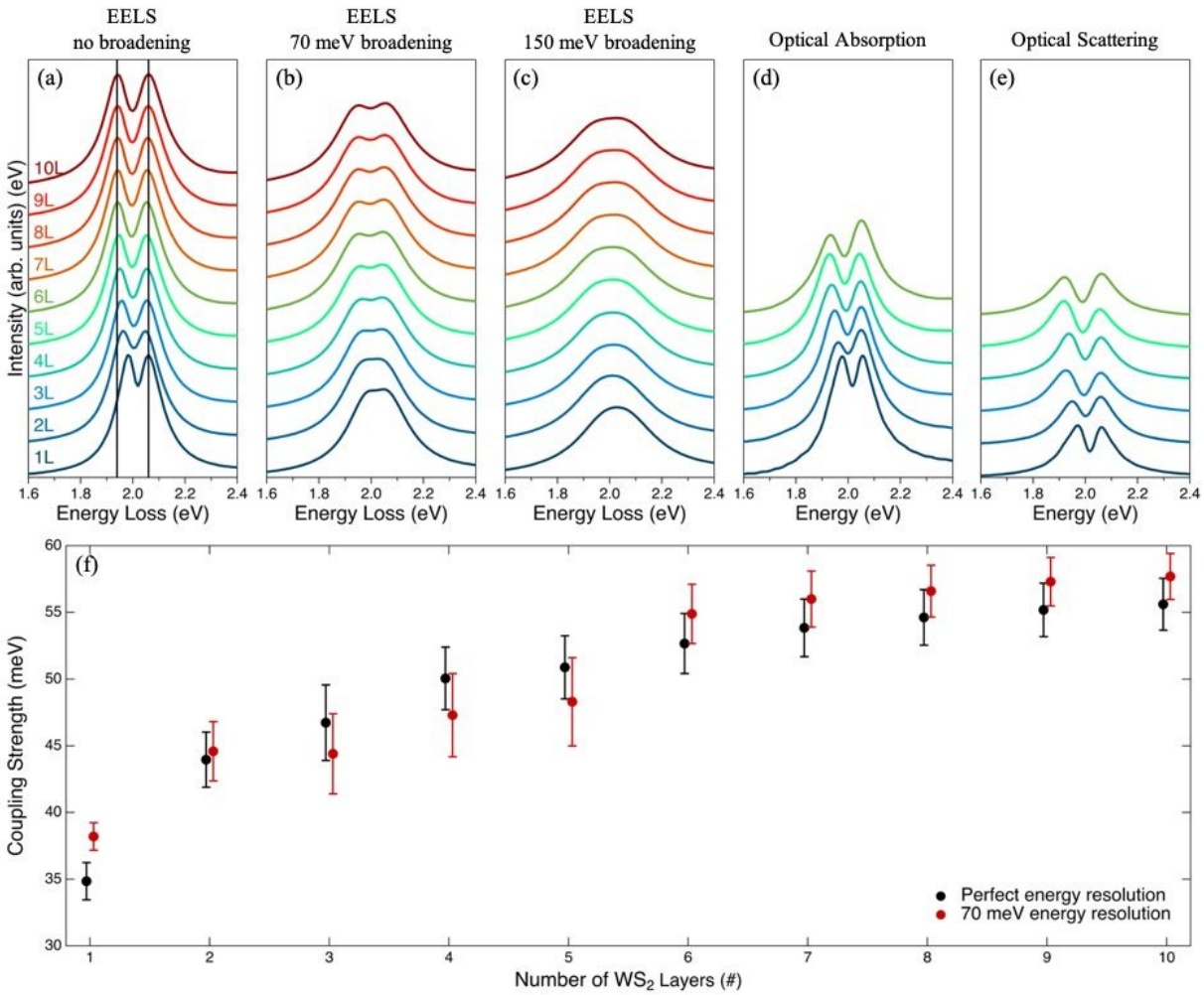

Figure S6. Simulated effect of number of WS_2 layers on Rabi splitting.
(a-c) Simulated EELS spectra from perfectly tuned coupled systems containing 1-10 layers of WS_2. Calculations are shown for (a) no (b) 70 meV and (c) 150 meV spectral broadening. The black vertical lines in (a) mark the apparent peak positions in the 10 layers spectra and help reveal the reduction in peak splitting magnitude with fewer number of WS_2 layers. These calculations predict that Rabi splitting should be observable for any WS_2 thickness if no spectral broadening is present. For 70 meV broadening, the splitting is predicted to be resolvable for WS_2 flakes thicker than 3-4 layers, but not for <3 layers. For 150 meV broadening, the splitting is completely unresolvable for any WS_2 thickness, highlighting the importance of using an instrument with sufficient energy resolution. In contrast, optical experiments resolve the peak splitting for any WS_2 thickness because of the superior spectral resolution. (d-e) Optical absorption and scattering simulations using the same perfectly tuned models that were used for the EELS calculations. The perfectly tuned models for each WS_2 thickness were determined for a 75 nm side length TNP by varying the TNP truncation height until the LP and UP display the same peak amplitude in the not broadened EELS calculations. (f) Plasmon-exciton coupling strengths (g) vs number of WS_2 layers, extracted from the EELS simulations in (a) and (b) using the coupled mode theory. These results show that reducing the EELS energy resolution should not affect the magnitude of the extracted g values. In addition, g saturates at >8 layers of WS_2, consistent with the saturation of the EELS peak splitting magnitude.

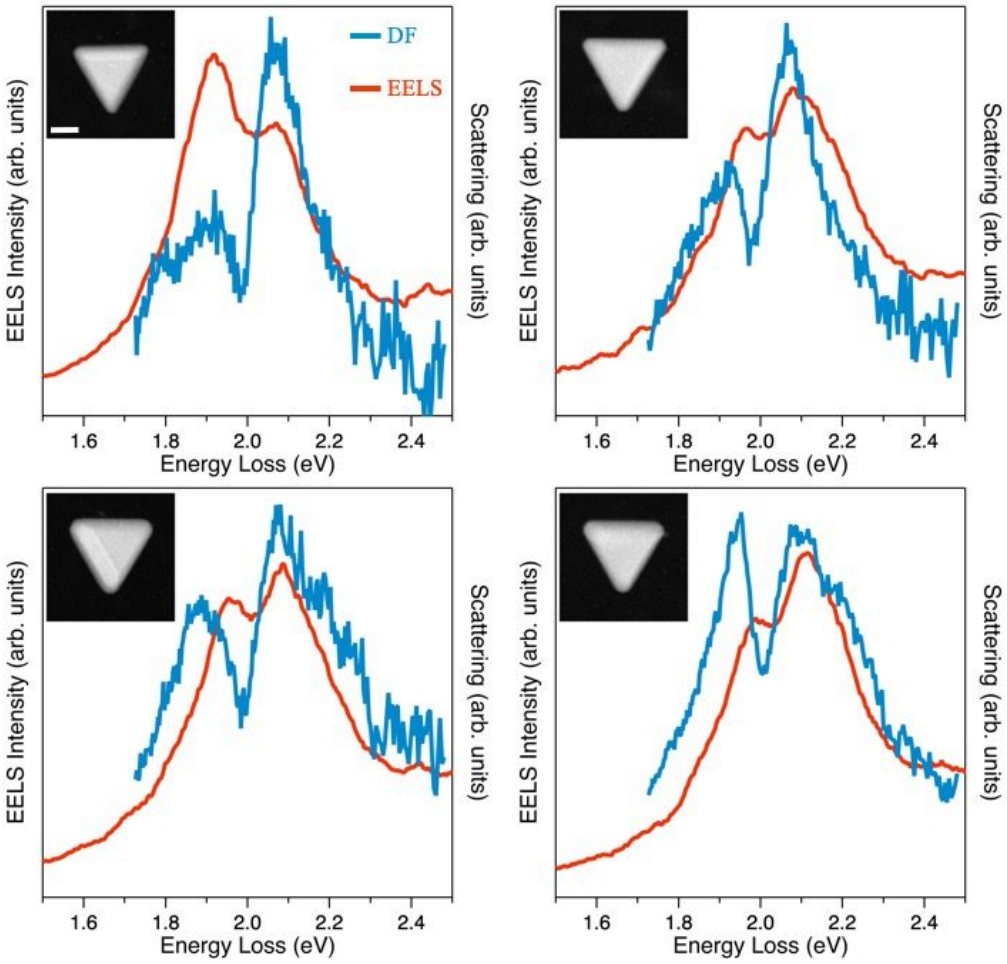

Figure S7. Additional correlation data from coupled systems.
Experimental EELS (red) and optical DF scattering (blue) of four coupled systems that exhibit different degrees of detuning and correlation. EELS spectra are acquired at a corner of the TNP. Each system is shown in the inset HAADF STEM image. The scale bar in the first HAADF STEM image is 30 nm and the scale is the same for every HAADF images.

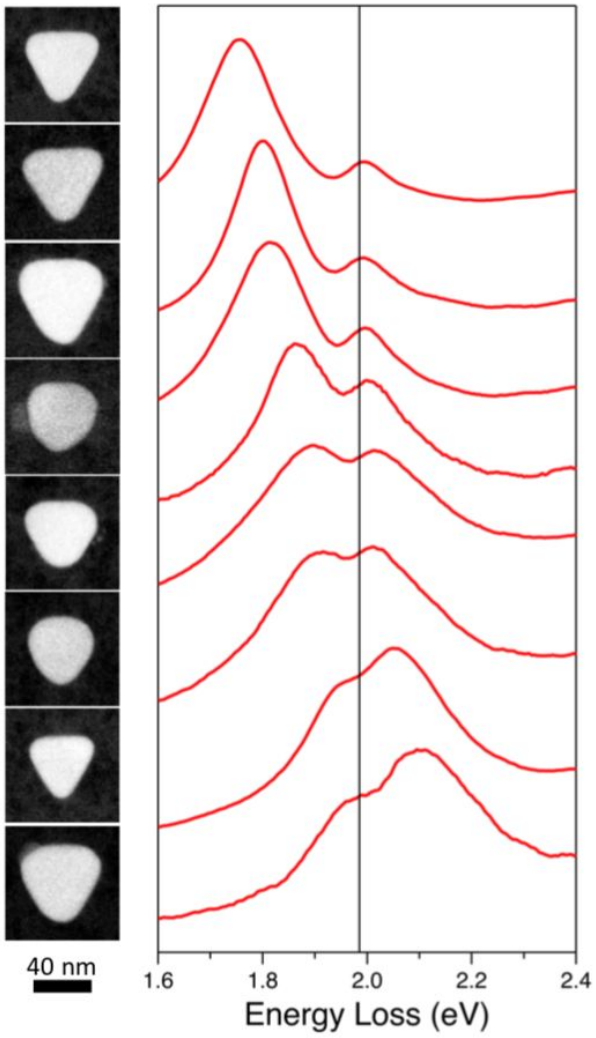

Figure S8. Polariton anti-crossing for absorption-dominated hybrid systems.
Experimental EEL spectra (red) from eight TNPs with shorter side-lengths compared to Figure 3b on the same WS_2 flake with various degrees of detuning. The black line shows the position of the WS_2 A-exciton measured using EELS. The top spectrum has a red-shifted LSP compared to the A-exciton, the middle spectrum is near the zero detuned condition, and the bottom spectrum has a blue-shifted LSP. HAADF STEM images of each TNP are shown in the inset images to the left. The 40 nm scale bar is applicable to all images.

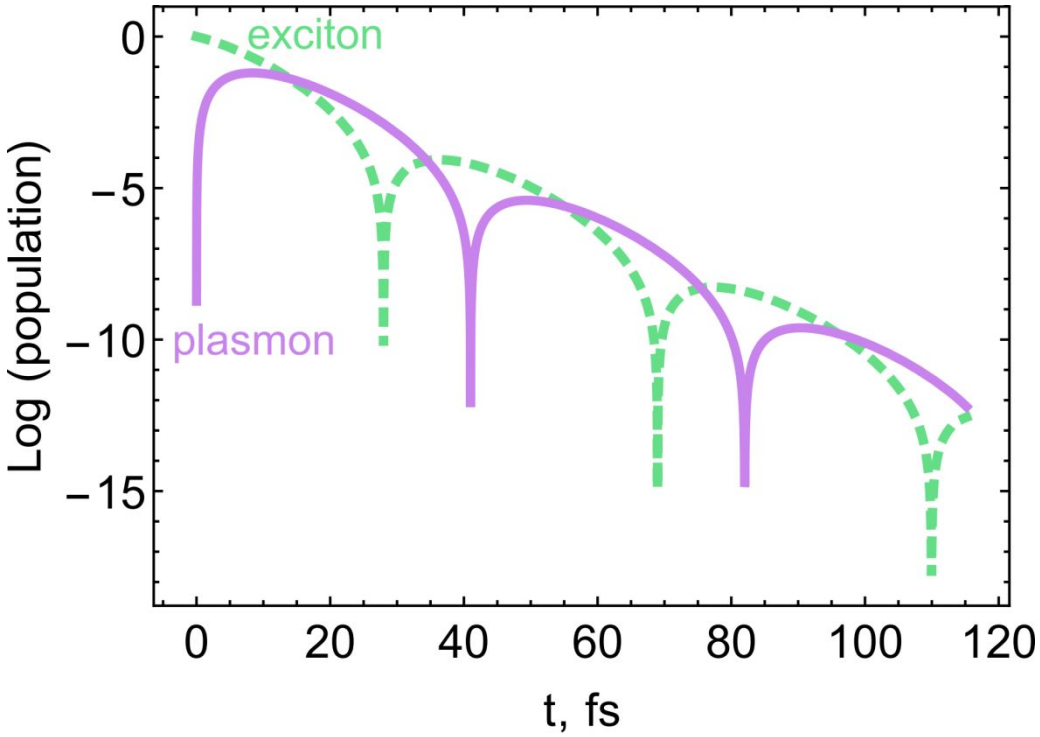

Figure S9. Simulated Rabi oscillation dynamics.
Rabi oscillations between a dipole LSP hosted by the Ag TNP and an exciton hosted by 6-layer WS_2 calculated with the use of the coupled mode theory assuming a 60 meV coupling strength, which was extracted from the EELS experiments. The transient populations were obtained by solving the dynamical equation of the coupled mode theory with the exciton being excited at t=0 in the absence of incident field.

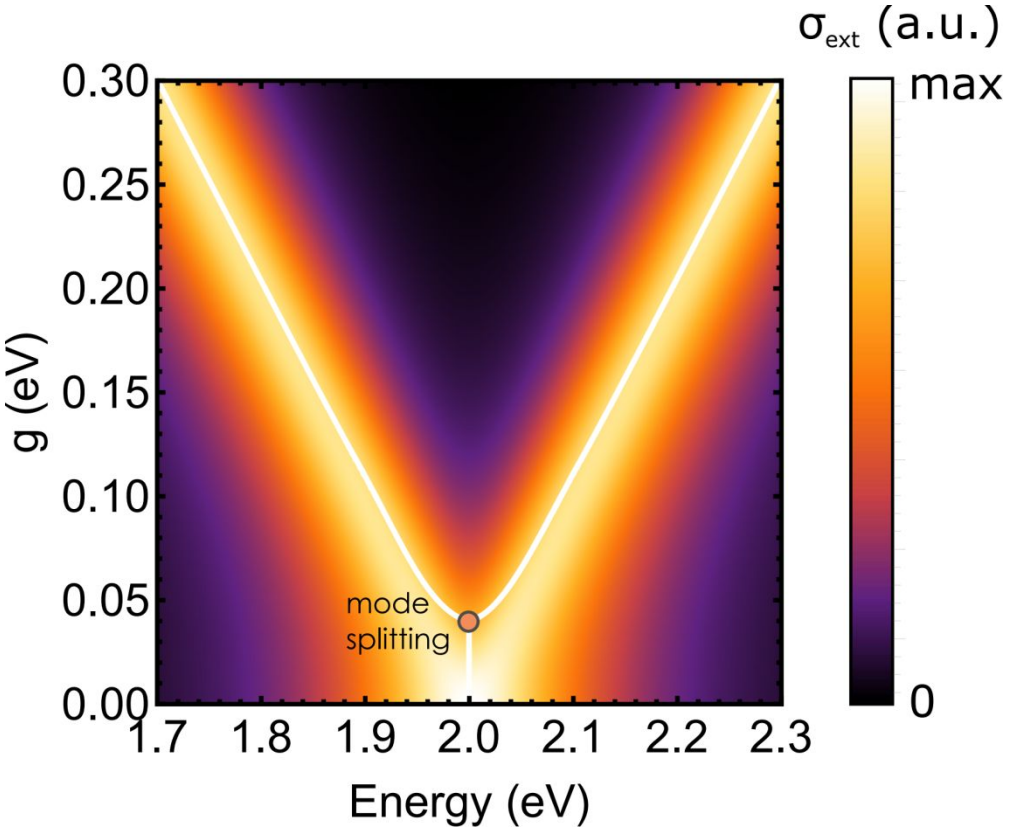

Figure S10. Relationship between coupling strength and observed splitting.
Extinction cross-section spectra of a generic coupled plasmon-exciton system as a function of the coupling strength g modeled with the use of the coupled-mode theory (see Methods) with $\gamma_{pl} = 210$ meV and $\gamma_X = 50$ meV. The white lines depict the eigenenergies of the coupled system experiencing the mode splitting at around $g \sim 0.04$ eV. One can clearly see that the distance between the two extinction maxima significantly overcomes the true Rabi splitting for small coupling strength values.

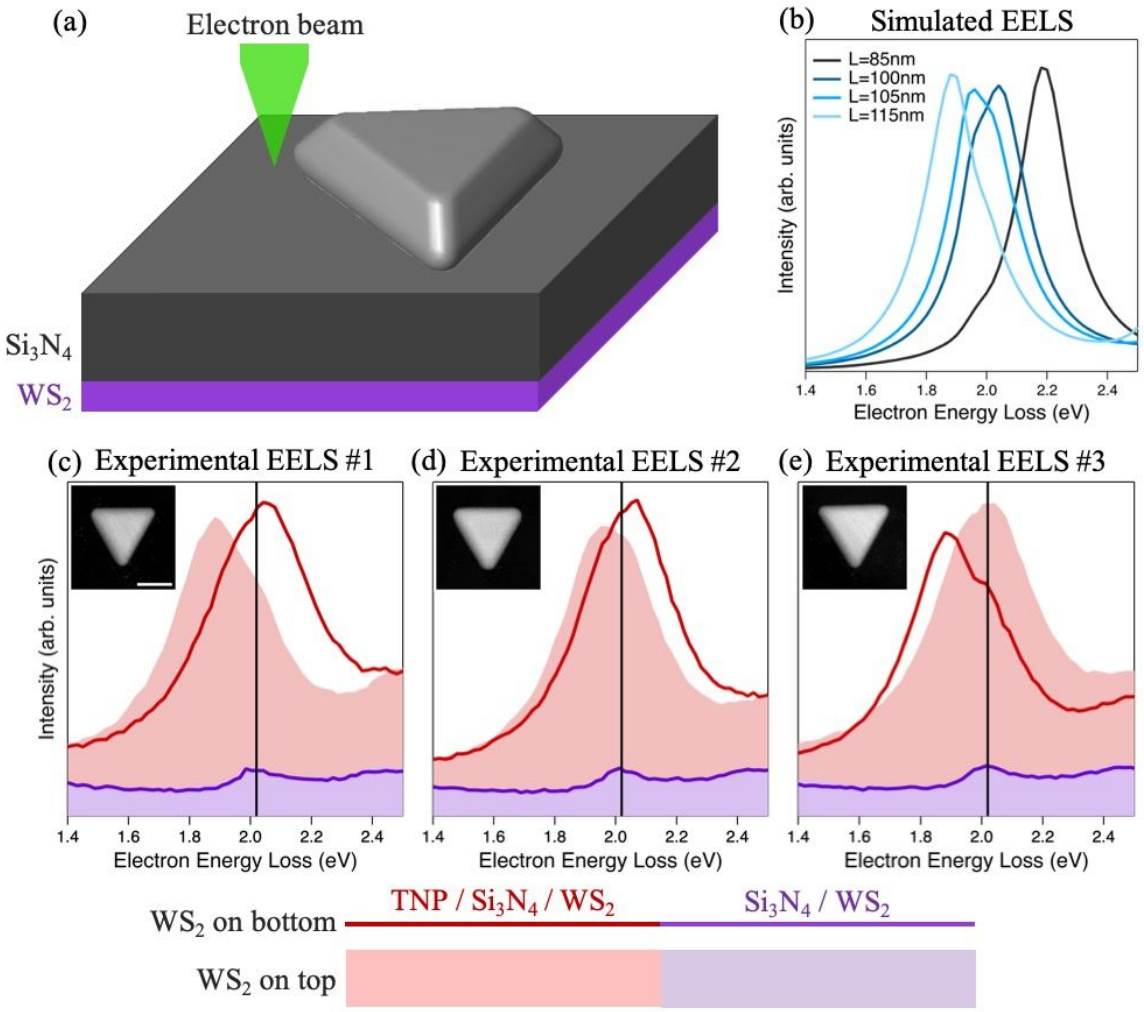

Figure S11. Spatially separating the Ag TNP and WS_2.
(a) Schematic of the experimental setup where the WS_2 and TNPs are spatially separated by the ~20 nm Si_3N_4 membrane, and the electron beam interacts with the TNP first and the WS_2 last. The samples were prepared by placing the WS_2 flakes on one side of the Si_3N_4 membrane and the Ag TNPs on the other side. This system was investigated to understand if this uncoupled system could produce peak splitting comparable to strongly coupled systems. (b) Simulated EELS spectra with no spectral broadening using a model where the TNPs and 8 nm thick WS_2 were placed on different sides of a 20 nm Si_3N_4 membrane. The 4 spectra are from TNP models with 85, 100, 105 and 115 nm side lengths. Different side lengths were used to study the effect of detuning the LSP and exciton. The simulations predict extremely minor peak broadening and shoulders, but there is no obvious mode splitting similar to what is theoretically predicted and observed from strongly coupled systems. (c-e) Three examples of experimental EELS spectra from spatially separated TNP and WS_2 systems. The purple spectra are from WS_2 a few hundred nanometers away from the TNP. The red spectra are acquired at the TNP corners. The line spectra were acquired when the sample was oriented such that the electron beam interacts with the WS_2 last. The filled spectra were acquired when the sample was oriented upside down, such that the electron beam interacts with the WS_2 first. The inset HAADF STEM images show each system. The scale bar in (c) is 50 nm and scaling is the same for all STEM images. The red spectra show signs of slight broadening but no mode splitting, which is similar to the predictions in (b). The changes in detuning of the same system in different orientation can be attributed to slight sample changes which can occur because the experiments were performed on different days.

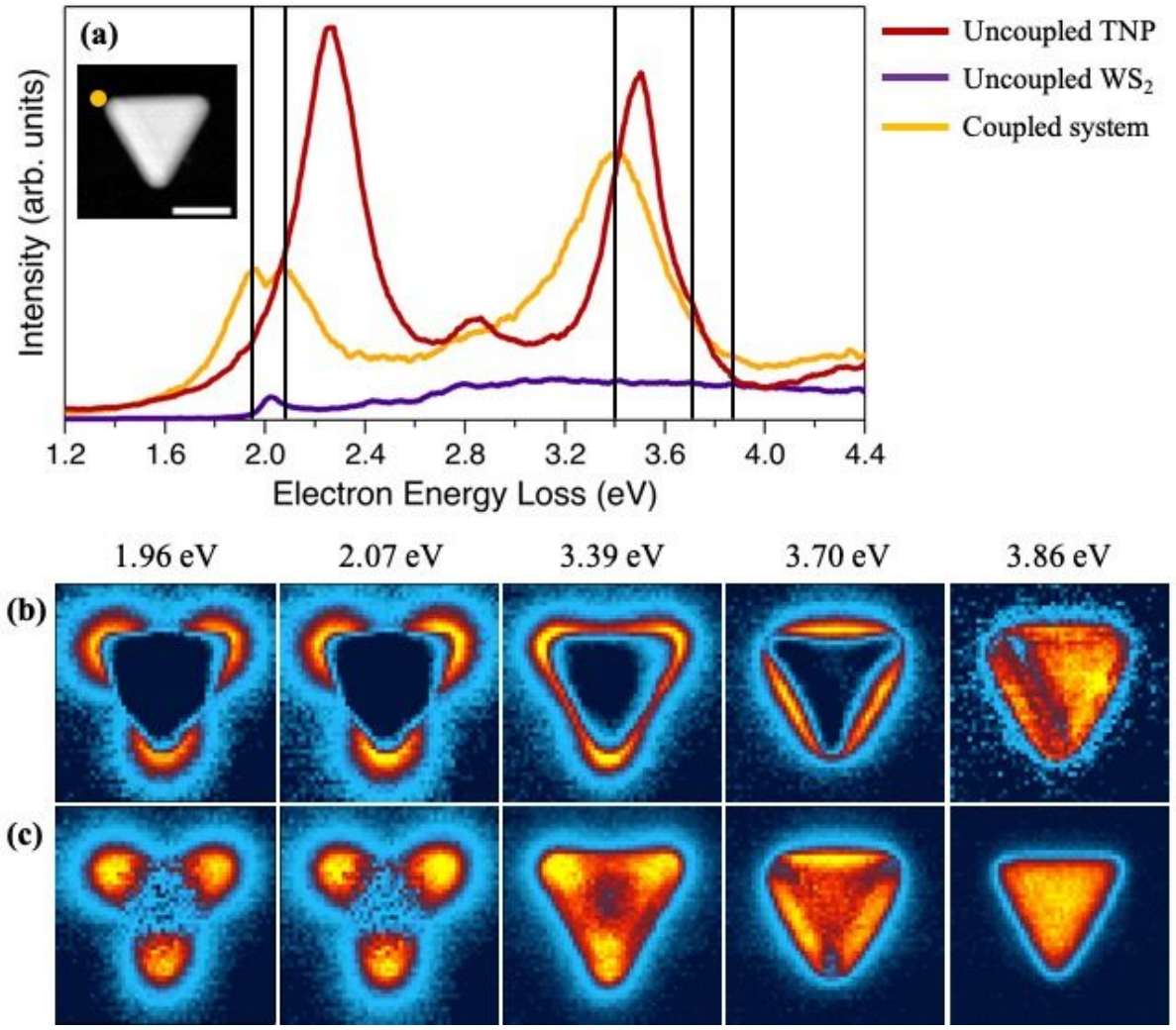

Figure S12. Additional EELS data from coupled system.
(a) EELS spectra from an uncoupled TNP (same as Figure S3, red curve), uncoupled 6 layers WS_2 (purple curve), and the same strongly coupled system that is shown in Figure 4 (orange curve). These spectra show the WS_2 exciton EELS excitation probability is more than an order of magnitude less than the uncoupled and coupled TNP LSP. The spectra also show the excitation probabilities of the LP and UP of the coupled system are reduced by a factor of two compared to the uncoupled TNP dipole LSP. The inset HAADF STEM image shows the coupled system and the corner that was measured in the orange spectrum marked by the orange circle. The scale bar is 50 nm. (b-c) Extracted maps from a (b) not-normalized and (c) normalized spectrum image (same spectrum images that are depicted in Figure 4) of the same coupled system shown in (a). The maps are extracted at 1.96, 2.07, 3.39, 3.70, and 3.86 eV, as marked by the black lines in (a). These energies were chosen because they show localization patterns in the EELS maps. The 1.96 and 2.07 eV maps correspond to the LP and UP. The 3.39 and 3.70 eV maps correspond to higher order modes. The 3.86 eV map corresponds to the bulk plasmon.

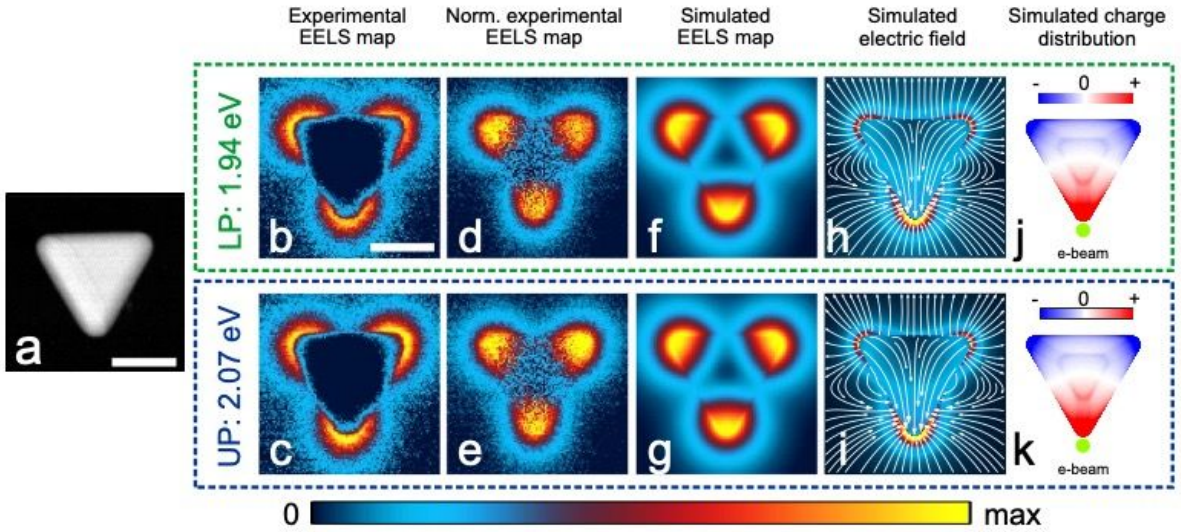

Figure S13. Experimental vs. simulated EELS data from coupled system.
(a) HAADF STEM image of the same coupled TNP – 6 layers WS_2 system shown in Figure 4. (b) and (c) are EELS maps of the coupled system shown in (a) extracted at the LP (1.94 eV) and UP (2.07 eV) energies, respectively, from a spectrum image that has not been normalized. (d) and (e) are EELS maps extracted at the LP and UP energies, respectively, from the spectrum image that has been normalized to the zero-loss peak height. (f) and (g) are simulated EELS maps extracted at the LP and UP energies respectively. (h) and (i) are FDTD simulated electric field distributions in the plane at the bottom of the TNP at the LP and UP energies, respectively, excited by a vertically polarized and normally incident plane wave. (j) and (k) are simulated surface charge density distributions at the LP and UP energies, respectively, excited by an electron beam passing along the green marker. The scale bars in (a) and (b) are 50 nm.